Journal of *Marine Science and Engineering*

MDPI

Article

Effects of Tsunami Shelters in Pandeglang, Banten, Indonesia, Based on Agent-Based Modelling: A Case Study of the 2018 Anak Krakatoa Volcanic Tsunami

Han Soo Lee [1,2,*], Ricard Diago Sambuaga [3] and Constanza Flores [1]

[1] Transdisciplinary Science and Engineering Program, Graduate School of Advanced Science and Engineering, Hiroshima University, 1-5-1 Kagamiyama, Higashi-Hiroshima 739-8529, Hiroshima, Japan; constanzaf.henriquez@gmail.com
[2] Center for the Planetary Health and Innovation Science (PHIS), The IDEC Institute, Hiroshima University, 1-5-1 Kagamiyama, Higashi-Hiroshima 739-8529, Hiroshima, Japan
[3] Department of Development Technology, Graduate School for International Development and Cooperation (IDEC), Hiroshima University, 1-5-1 Kagamiyama, Higashi-Hiroshima 739-8529, Hiroshima, Japan; ricarddiagos@gmail.com
* Correspondence: leehs@hiroshima-u.ac.jp; Tel.: +81-82-424-4405

Abstract: On 22 December 2018, the volcanic eruption of Anak Krakatoa in the Sunda Strait, Indonesia, triggered a tsunami causing 437 deaths. The highest death toll and the second highest number of damaged houses were recorded in Panimbang. This study proposes optimum evacuation shelters to reduce the mortality rate. A digital elevation model (DEM) and information dataset are used. The suggested horizontal evacuation shelters (HESs) are places of worship, schools, and government offices. Multimodal agent-based modelling (ABM), to analyse the sensitivity of parameters and the effect of vertical evacuation shelters (VESs) under multiple scenarios, is presented for the volcanic tsunami in December 2018. A tsunami hazard map is created by combining relative weights and parameter scores for topography, slope, and the distance from the shoreline and rivers. In the ABM results, the transportation mode choice depicts a significant decrease in the number of casualties. The mortality rate is sensitive to the milling time caused by delay time τ and agent decision-making time σ. VESs are proposed at the hot spots based on the location of deaths in the sensitivity tests and the high and very-high risk zones in the hazard map. As a result, combinations of VESs and HESs show a decrement in the number of deaths by 1.2–2 times compared to those with HESs only. The proposed VESs in the study area have a significant positive impact on decreasing the mortality rate.

Keywords: vertical shelters; evacuation; agent-based model; landslide; Anak Krakatoa; volcano eruption

check for updates

Citation: Lee, H.S.; Sambuaga, R.D.; Flores, C. Effects of Tsunami Shelters in Pandeglang, Banten, Indonesia, Based on Agent-Based Modelling: A Case Study of the 2018 Anak Krakatoa Volcanic Tsunami. *J. Mar. Sci. Eng.* **2022**, *10*, 1055. https://doi.org/10.3390/jmse10081055

Academic Editor: Efim Pelinovsky

Received: 7 July 2022
Accepted: 29 July 2022
Published: 31 July 2022

Publisher's Note: MDPI stays neutral with regard to jurisdictional claims in published maps and institutional affiliations.

Copyright: © 2022 by the authors. Licensee MDPI, Basel, Switzerland. This article is an open access article distributed under the terms and conditions of the Creative Commons Attribution (CC BY) license (https://creativecommons.org/licenses/by/4.0/).

1. Introduction

Indonesia is an archipelagic country that has a high potential for natural hazards due to its location in the "ring of fire" among three large tectonic plates, the India-Australia, Pacific, and Eurasian plate. Indonesia often experiences volcanic eruptions and earthquakes with a high potential for tsunamis. Based on statistical data on historical tsunami events in Indonesia (Table S1 in Supplementary material), the high incidence, the number of deaths, and losses due to tsunamis in Indonesia need special attention in the future so that those figures can be reduced depending on the level of preparedness.

Tsunami preparedness is very important in the effort to prevent future disasters. In tsunami preparedness, many aspects must be considered. In Indonesia, many efforts have been employed with regard to tsunami preparedness, yet further improvement is needed [1–5]. One of the main problems with tsunami preparedness in Indonesia is related to the lack of socioeconomic resources such as occupations, types of housing, level of education, opportunity for tsunami evacuation drills, exposure to disaster-related information, and so on, for local villagers. Most settlements are generally located near the coastline without proper

spatial planning. Moreover, houses in coastal areas are generally constructed of wood, with concrete bricks being used only for the walls, and poorly constructed concrete buildings. In other words, those houses and buildings are vulnerable to tsunamis. Furthermore, tsunami drills are needed for the local population, especially for those who live in high tsunami-risk coastal zones.

Tsunami drills are important for increasing the awareness of people and increasing their knowledge of the evacuation process. Tsunami awareness is also critical for carrying out a successful evacuation timely so that the number of deaths can be decreased. The problem with tsunami drills is that some areas in high-risk zones have never taken part in tsunami drills; additionally, not all of the population has participated in a tsunami drill. Adiyoso and Kanege (2012) [6] reported a case study in which a curriculum based on disaster issues for school children could be adopted to reduce disaster risk. Such a curriculum is important because teachers and students play an important role in raising public awareness, spreading correct knowledge about disasters, and promoting behavioural preparedness for disasters in the wider community. In addition, an engineering tool such as an integrated simulation system for storm surge, inundation, and evacuation can be very useful to support disaster education and outreach [7].

Early warning systems and evacuation routes and shelters play a major role in a preventive action against tsunami disasters in Indonesia. The Indonesian government has provided a tsunami warning system that consists of public broadcasting, tsunami hazard maps, and tsunami evacuation maps. The Indonesian government has also released an information guidebook—Tsunami Early Warning for Broadcasting Institutions in Indonesia [8]. This guidebook discusses guidelines for providing tsunami information to the public via TV, radio, short message services (SMSs), websites, and social media. It addresses detection and analysis instruments for early warning as well as the roles and responsibilities of institutions in the tsunami early warning communication chain.

In the case of the Sunda Strait volcanic tsunami in December 2018, no appropriate tsunami warning system was provided by the authorities [9]. The tsunami warning system in Indonesia should be extended to anticipate nonseismic tsunamis, such as underwater landslides and volcanic process-driven tsunamis. For nonseismic tsunamis, the government has not released a tsunami evacuation map and route, and appropriate field survey-based evacuation shelters have not been provided. The authorities released an evacuation map only after the event in 2018. In the 2018 tsunami events, when the tsunami occurred and people needed to evacuate to high-elevation areas or hills, public facilities such as mosques, government offices, and schools could not be used as a temporary evacuation shelter (TES).

The official TES provided by the authorities in the Pandeglang District, Java Island, Indonesia, is the only TES in the flat coastal area located in the Labuan subdistrict. Consequently, in the case of a tsunami, there is nowhere for people in Panimbang to evacuate. As noted above, early evacuation is one of the most critical and effective methods for saving lives. Based on Ashar et al. (2014) [1], vertical evacuation is defined as the act of individuals saving themselves by heading toward higher ground, either on a hill (natural shelter) or in a multistory building. Since the Panimbang area is generally flat and does not have a distinct higher ground, multistory buildings should be considered vertical evacuation shelters (VESs). VESs are considered temporary, accommodating evacuees for approximately 2–3 h before they move to a tsunami evacuation centres in a safe zone.

Since the 2004 Indian Ocean tsunami, numerous case studies on tsunami disaster awareness and preparedness have been discussed and reported [10–15]. However, there are few studies applying the agent-based models (ABMs) for evacuation process investigation, evacuation planning, city planning, and risk management [10,11,15].

Based on the background above, this study aims to propose an optimized evacuation plan with (i) evacuation shelters in the study area, (ii) the time required to reach the shelters, and (iii) death toll and mortality rate estimation, based on the comprehensive simulation results of an ABM under various scenarios. In addition, it also demonstrates the effects of various factors in agent behaviour on death toll estimation.

2. Materials

2.1. Study Area

On 22 December 2018, a tsunami caused by the volcanic eruption and the partial collapse of the Anak Krakatoa volcano occurred in the Sunda Strait, Indonesia [16–18]. Figure 1 illustrates the location of Anak Krakatoa in the Sunda Strait. The Sunda Strait connects the islands of Java and Sumatra (Banten Province, Java, to Lampung Province, Sumatra) and connects the Java Sea to the Indian Ocean. Anak Krakatoa (Child of Krakatoa) is a volcanic mountain located in the Sunda Strait. Anak Krakatoa emerged from below the surface of the sea in 1927 [19] following a large eruption of Mount Krakatoa in 1883, one of the largest volcanic eruptions in the world. The 1883 tsunami caused by the large eruption of Anak Krakatoa resulted in 36,000 deaths, and it generated a pyroclastic flow of more than 5 km^3, with an average discharge rate of 107 m^3/s [20]. Since 1927, Anak Krakatoa has erupted frequently, with eruptions typically strombolian to vulcanian in style, characterized by small explosive eruptions, with columns reaching 1 km in height, and pyroclastic and lava flows [21]. Volcanic activity began to start again in June 2018 and lasted until December 2018. The height of Anak Krakatoa has increased by 4–6 m/year due to of eruptions.

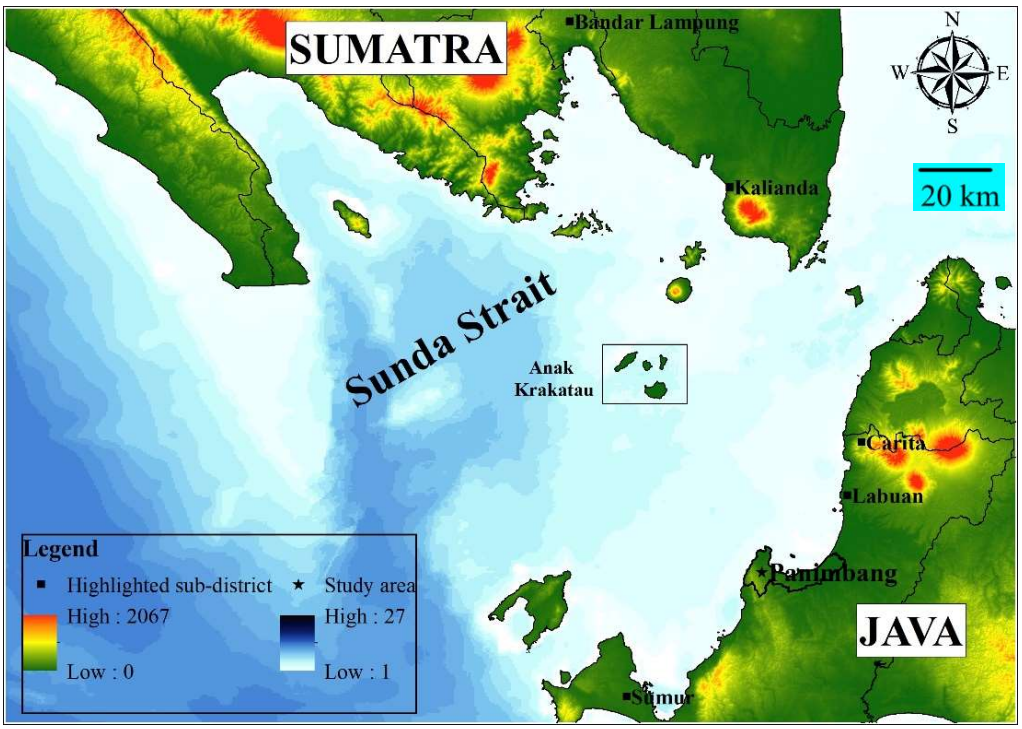

Figure 1. Location of Anak Krakatoa in the Sunda Strait between Java and Sumatra Islands, Indonesia.

The official number of casualties reported was 437 deaths, 31,942 injuries, and 10 still missing [22,23]. The total numbers of casualties in Banten Province and Lampung Province were 317 and 120, respectively. The Panimbang subdistrict located in Pandeglang, Banten, was chosen as the study area in this research. It has a total population of 51,692 in the Panimbang subdistrict and the highest number of deaths (129 out of 295) in the Pandeglang District due to the December 2018 Anak Krakatoa tsunami. This subdistrict also had the third highest number of damaged houses in Pandeglang [24].

The only official TES in Pandeglang is in Labuan, and no TES is provided in Panimbang. The TES in Labuan is an approximately 20 m tall vertical concrete structure with open space on top for shelter, with no roof, and is located approximately 300 m from the shoreline with easy access from the main road. In the 2018 tsunami event, people were evacuated to their nearest hill or highland area. According to the local authorities, the Regional

Disaster Management Authority (BPBD) of Pandeglang District, no evacuation route map was released until after the 2018 tsunami event. They recommended the location of hills or highland areas as an evacuation area and only provided signs for tsunami evacuation locations. These actions were an insufficient standard for the evacuation process. Since the Panimbang subdistrict is in a high tsunami-risk zone, more research is needed to provide appropriate and optimum evacuation routes and shelters.

2.2. Datasets

There are five main components/datasets used for agent-based modelling: the population distribution, road network, tsunami inundation data, locations of evacuation shelters, and casualty model. Each component is described in detail below.

2.2.1. Population Distribution

The population dataset as a residential location shapefile from the government is imported into the GIS spatial analysis tool. These residential locations are counted as agents in the model. As described previously, the total population in the Panimbang subdistrict is 51,692 [24] and is presented in Figure S1 in the Supplementary Material. The total population and the Panimbang residential area are used as an agent's initial location in the model. The percentages of males and females in this subdistrict are 51.18% and 48.81%, respectively.

The Panimbang population data are divided into 16 age groups in 5-year increments (0–4 to 75+). In this study, however, these data were divided into only 3 groups: 31.31% children (age 0–14), 51.43% adults (age 15–49), and 17.26% elderly individuals (age 50–75+). Sex was not considered in this study. In the simulation, the total number of agents that are modelled is 5169 for considering computation load, with 1 agent representing 10 residents. In a realistic situation, people respond to a hazard differently based on their knowledge, educational background, physical condition, etc. However, it is assumed that all agents are subjected to the hazard in the same fashion. In other words, they choose their destination, route, transportation mode, and immediacy of evacuation regardless of their knowledge and familiarity with the area.

2.2.2. Road Network

The main road network, also retrieved from the government statistics, is imported into the model as a shapefile. It is assumed that all agents (pedestrians, cars, and motorcycles) follow the network and go to their nearest shelter. The total percentage of motorcycles in Indonesia is 81.8% and that of cars (cars, buses, and lorries) is 18.2% [25]. These vehicle percentages in Indonesia are applied to represent the vehicle percentages in the Panimbang subdistrict. Pedestrian shortcuts involving the use of small roads are not considered in the model. In this simulation, the entire network is composed of one-way, one-lane streets with a maximum speed limit of 40 km/h. This assumption is based on the maximum speed limit in the study area and field observations.

Based on the assumptions, the road network is imported into the model as a link. At the beginning of the simulation, all agents head to the nearest link (nearest road network) where they calculate the value of decision-making probabilities to evacuate on foot, by car, or by motorcycle.

2.2.3. Tsunami Inundation

The inundation data used in this study are based on the detided waveform records of the Anak Krakatoa volcanic tsunami that occurred on 22 December 2018 [26]. The tide gauge observations are available at six locations: Marina Jambu, Ciwandan, Panjang, Kota Agung, Bengkunat, and Binuangeun (Figure S2). In this study, the records from the nearest tide gauge at Marina Jambu to the study area are used. Figure S3 and Table S2 show the detided waveforms of the Marina Jambu tide gauge. The tsunami wave height starts to

increase 32 min after the time of the eruption. The first wave arrived at the coastline 34 min after the eruption and reached its maximum height (1.35 m) 39 min after the eruption.

In the simulation, the speed and direction of the flow are neglected, and tsunami inundation is considered as the flow depth. The bare-earth model is used as a base layer in this model. The bare-earth model, also known as the digital elevation model (DEM), is an unmodified or original dataset, which means that the data are supposedly free of vegetation, buildings, and other nonground objects [27]. Even though this model uses bare-earth elements, the underlying assumption is conservatively valid.

2.2.4. Shelter Location

Since no TES is provided in Panimbang, public buildings such as schools, government offices, and worship facilities are proposed as shelters in this study. This shelter information is also imported as a shapefile. All shelters are assumed to structurally withstand earthquake and tsunami forces [28,29] without the maximum capacity.

In addition, vertical evacuation shelters (VESs) are proposed in this study. These additional shelters are used as a simulation scenario. The effect of VESs is compared to the result of a simulation in which only horizontal evacuation shelters (HESs) are used [30].

2.2.5. Casualty Model

In this study, the casualty model is simplified. Basically, if a wave with a height of H_c or more touches an agent, it will be considered a cause. This study makes this assumption because calculating the mortality rate can be highly complicated due to the variations in a person's age, gender, physical state, and transportation mode [31]. This assumption might not reflect the actual mortality rate, however, H_c can still be used to reflect the vulnerability of evacuees to the inundation force. In the simulation, H_c is conservatively set to 0.5 m. At this wave height, it is assumed that it is difficult for agents to evacuate or that they can no longer move to the nearest shelter and are thus counted as deaths.

3. Methodology

3.1. NetLogo and Model Setups

The tsunami evacuation modelling uses an ABM approach coded in NetLogo. NetLogo involves high-level integrated modelling through an agent-based programming language [32]. It is an open-source software/platform and offers flexibility in modelling agent interactions and heterogeneous decision-making [32].

In ABM, for creating evacuation modelling, most of the difficulties are caused by the interaction between agents that capture the emergent behaviour of the whole system. That is, integrating agent-agent interactions, agent-environment interactions, and interactions between an agent and any physical, psychological, or social condition is complex [32].

In this study, the simulation focuses only on the consequences of tsunami hazards. It does not include the consequences caused by debris flows and traffic accidents in emergencies. According to [33], more than 90% of deaths in the 2011 Tohoku tsunami disaster were attributed to inundation. It is assumed that all agents are autonomous and heterogeneous and that their surrounding environment and interactions directly influence their choices. To simplify agent behaviour, agents are assumed to decide to evacuate, and there is no option for staying. In this case, agents can choose only one transportation mode (walking, cars, or motorcycles). They cannot switch their transportation mode during the evacuation process. A detailed explanation regarding the modelled behaviour is presented in the next subsections.

Figure 2 illustrates the NetLogo interface used in this study. As shown in Figure 2, the light blue colour represents the sea-level height, and it becomes darker when the water level increases. The total number of agents modelled in this simulation is 5169. There are five different agent types in this model, i.e., those who choose to evacuate by walking (children, elderly people, and adults) and those who choose to evacuate by vehicle (cars and motorcycles). A large circle in the interface represents the locations of shelters used in this

study. The red colour represents deaths caused by the tsunami. In this model, we can set up several parameters as inputs for tsunami evacuation, such as the shelter type, decision-making probabilities, critical depth (water level limit for an agent to evacuate), walking speed and sigma, vehicle speed, acceleration, deceleration, and milling time parameters (delay time and variations in the departure time). The output produced in this simulation is the percentage of deaths and evacuated people and the evacuation time.

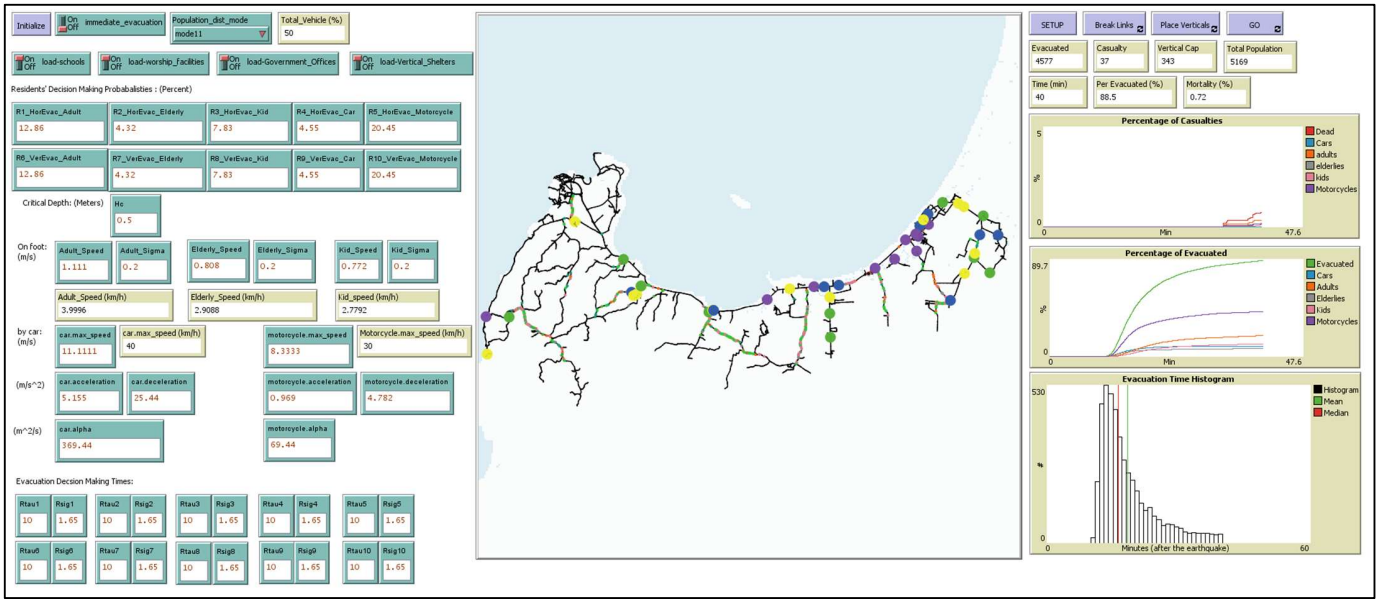

Figure 2. ABM modelling interface using NetLogo used for the tsunami evacuation process in the Panimbang subdistrict. Brown circles indicate the initial population (agents), schools in yellow, worship facilities in green, government offices in blue, and VESs in purple.

3.2. Optimization Algorithm

Model optimization is related to the implementation of pathfinding algorithms correlated to agent decisions. Several shortest path algorithms have been studied, such as the A-star (A*), Dijkstra, and greedy algorithms.

The Dijkstra algorithm tries to find the shortest path from the starting node to every node [34]; hence, it can determine the shortest path to the goal. The implementation of the Dijkstra algorithm considers only the real cost. This algorithm can assist in finding the shortest path from the starting point to the goal if the edges do not have any negative cost. However, it tends to take longer for calculations since it calculates every vertex until it obtains the shortest path to the goal.

The greedy algorithm uses a heuristic for estimation to reach the goal, reducing the search cost [35]. It performs some estimations of how far it is for any vertex to reach the goal. The main advantage of this algorithm is that it runs more quickly than the Dijkstra algorithm because the greedy algorithm uses a heuristic function to guide its path towards the goal expediently. However, this algorithm cannot guarantee that it will find the shortest path from the starting node to the goal. The problem with this algorithm is that it tries to move towards the goal even if a path is not the right path since the algorithm considers only the cost of arriving at the goal from the starting node and ignores the cost of the path.

The A* algorithm simply combines both the Dijkstra and greedy best-first-search algorithms [36]. As a result, it can perform as fast as the greedy algorithm because it uses a heuristic to guide itself and finds the shortest and optimum path, just as the Dijkstra algorithm does. The main idea of this algorithm is that it combines the information that the Dijkstra algorithm uses (calculates the vertices that are close to the starting point) and the heuristic approach that the greedy algorithm uses (calculates the vertices that are close to

the goal). In general, the terms used when discussing the A* algorithm are indicated by Equation (1).

$$f(n) = g(n) + h(n) \quad (1)$$

where $g(n)$ represents the exact cost of the path from the initial location or starting node to the goal and $h(n)$ represents the heuristic estimated cost from vertex n to the goal [36]. In another case, when $h(n) = 0$, the A* algorithm is the same as the Dijkstra algorithm because the heuristic estimated cost is not considered. In this study, the A* algorithm is implemented. It is assumed that the agent has already calculated the shortest and optimum path from the initial location (starting node) to the goal (closest shelter). Traffic congestion is not considered.

3.3. Model Behaviour

Figure 3 illustrates examples of the model behaviour overview. In this model, the simulation starting from t = 0 min and finishing at t = 60 min represents the initial collapse due to the volcanic eruption and the end of the evacuation scenario. The time step was one minute and the grid size was 83 m. It is assumed that there was no evacuation process during the volcanic eruption. An agent's initial location in Figure 3a represents the actual resident's location.

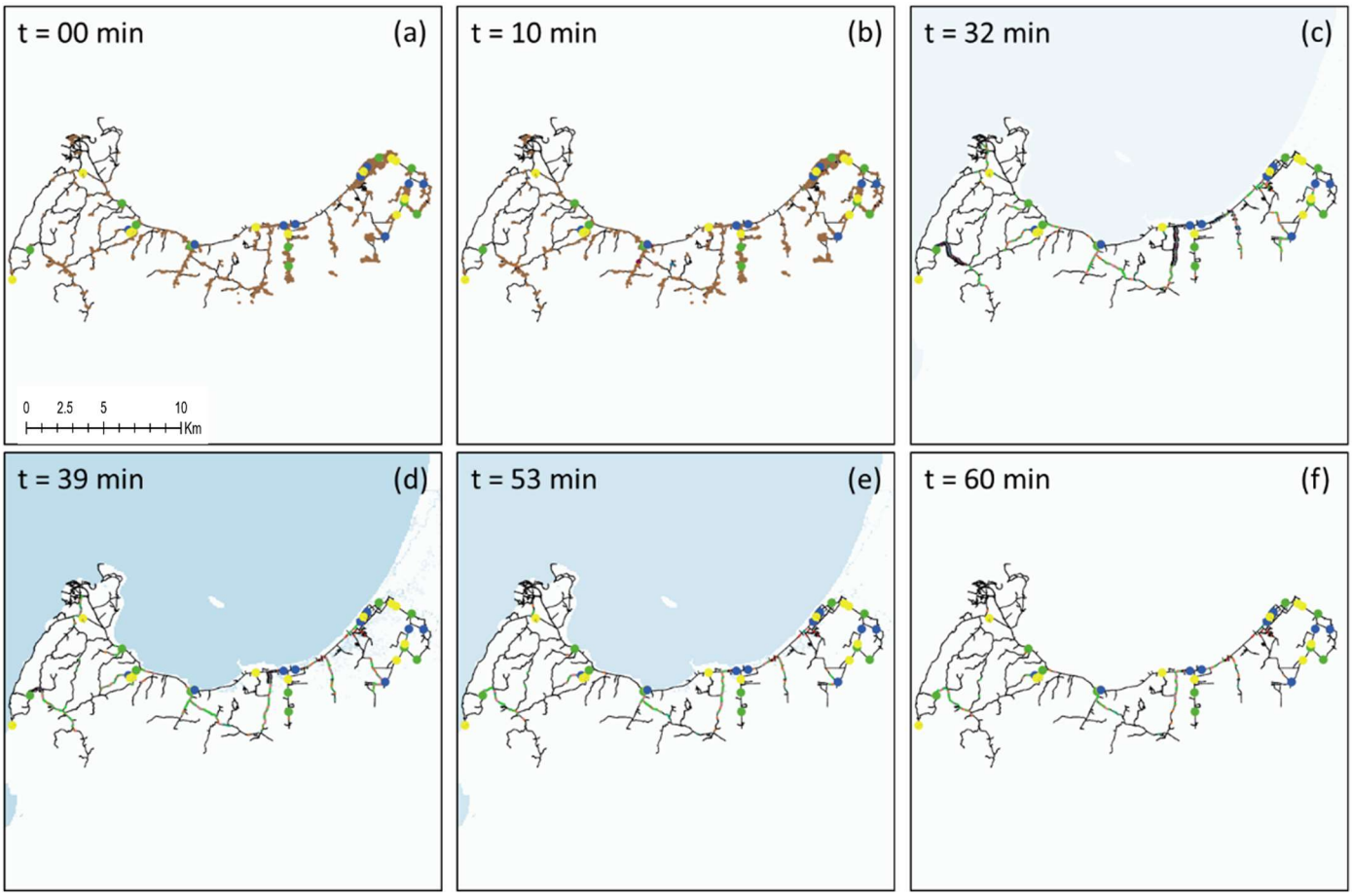

Figure 3. Model behaviour overview at different simulation times, t = 0 (**a**), 10 (**b**), 32 (**c**), 39 (**d**), 53 (**e**), and 60 (**f**) minutes, with the initial population (agents) indicated by brown circles, schools in yellow, worship facilities in green, government offices in blue, and VESs in purple.

Figure 3b shows at t = 10 min that the evacuee has started his or her evacuation to his or her nearest shelter. Agents can evacuate via different transportation modes, by foot, car, or motorcycle. Agents change colour and shape depending on their transportation modes.

At this stage, the initial colour of agents starts to change to orange, representing adults who evacuate by foot, grey, representing elderly individuals who evacuate by foot, and pink, indicating children who evacuate by foot. The sky colour represents cars and motorcycles (the car shapes and bike shapes in the model). However, many agents are delayed and are still at their initial location.

Figure 3c shows approximately at t = 32 min that the first tsunami wave arrived at the coastline. Figure 3d shows the evacuation process at t = 39 min. At this stage, the tsunami wave height reached the maximum (1.35 m). Fatalities or casualties occurred when the inundation level exceeded H_c (0.5 m), represented by red agents. Figure 3e shows that the total deaths increased at t = 53 min, while the inundation level increased again to 0.95 m. In Figure 3f, the simulation is completed at t = 60 min. At the end of the simulation, the total number of evacuees and deaths are counted and used to consider optimum evacuation shelters. The tsunami height waveform over time observed at the Marina Jambu tide gauge is shown in Figures S2 and S3 in the Supplementary Material.

3.4. Agent Decisions

3.4.1. Transportation Mode Choice

The transportation mode choice involves five agent types under 11 mode choices. Each mode is related to the combination of vehicle usage and the population distribution divided by age groups. It is assumed that all agents are located at ground level and outside. In other words, they are not in their vehicle or building. The transportation modes are divided into moving by foot/walking (adults, children, and elderly people), motorcycles, and cars. Each agent can make only one of the following choices. In other words, agents who use cars and motorcycles are counted as one agent. Another assumption is that cars and motorcycles are located nearby. The time that it takes to go to a car and motorcycle is modelled and accounted for in the milling time section. To simplify the model, it is assumed that all agents know the shortest and most efficient route to the nearest shelter from their initial location.

The main principle of the transportation mode choice is that in mode choice 1, the entire population evacuates by foot with 0% vehicle use, with the modes continuing at 5% increments of vehicle use and with a simple ratio for each decision until 50% vehicle use is reached in mode choice 11 (Table 1).

Table 1. Transportation mode choice ratio.

Agent Type	Mode 1	Mode 2	Mode 3	Mode 4	Mode 5	Mode 6	Mode 7	Mode 8	Mode 9	Mode 10	Mode 11
Adults	51.42	48.85	46.28	43.71	41.14	38.57	35.99	33.42	30.85	28.28	25.71
Elderly people	17.26	16.40	15.53	14.67	13.81	12.95	12.08	11.22	10.36	9.49	8.63
Children	31.32	29.75	28.19	26.62	25.06	23.49	21.92	20.36	18.79	17.23	15.66
Cars	0.00	0.91	1.82	2.73	3.64	4.55	5.46	6.37	7.28	8.19	9.10
Motorcycles	0.00	4.09	8.18	12.27	16.36	20.45	24.54	28.63	32.72	36.81	40.90

3.4.2. Shelter Choice

In this study area, evacuation shelters are not provided. An official evacuation shelter provided by the government is located in the Labuan subdistrict, Pandeglang. Therefore, public buildings, such as schools, government offices, and worship facilities, are proposed as shelters in the simulation. It is assumed that each shelter has an unlimited capacity. In the shelter choice, the main principle is to analyse the ratio of a single shelter to the total number of evacuees and deaths. Regarding each shelter choice, there are 14 schools, 10 worship facilities, and 9 government offices.

3.4.3. Milling Time

Milling time is a critical aspect of evacuation modelling for a near-field tsunami [37]. The preparation time is short in the case of a near-field tsunami. According to [38,39], the reliability and quality of the messages conveyed regarding the evacuation process,

the public response to the messages, and the performance of decision-makers affect the evacuation milling time. Many studies have discussed the preparation time for natural hazards with long preparation times [40] and rapid onset, such as tsunamis, which still need to be examined thoroughly [39]. Milling time also greatly impacts the formation and evolution of bottlenecks and traffic congestion, affecting the mortality or casualty rate [30]. Mas et al. (2012) [41] suggested considering the evacuation preparation time to calculate the evacuation process and the departure time, *P(t)*, presented in a Rayleigh distribution [30].

To abstractly consider the decision-making process, the values of τ and σ are reasonably calibrated, and the milling time is randomly drawn from the Rayleigh distribution based on Equation (2) [40].

$$P(t) = \begin{cases} 0 & 0 < t < \tau \\ 1 - e^{-(t-\tau)^2/(2\sigma^2)} & t < \tau \end{cases} \quad (2)$$

t represents the departure time after an earthquake or initial disturbance in minutes, τ represents the minimum preparation time to evacuate, and σ is the spread of the departure time. The larger σ is, the larger the tail of the later departure time distribution. According to ref. [30], slight increases in τ and σ will lead to an increase in the mortality rate. Immediate evacuation is an important aspect that can reduce the mortality rate. It is assumed that immediate evacuation is characterized by τ = 1 min and σ = 0.5, which means that 99% of all agents start their evacuation from 1 min to 2 min and 30 s. Table 2 shows the percentage of different departure times for different values of σ (variations in departure time), and it is assumed that τ = 0.

Table 2. Required time (min) for agents to initiate an action as a function of σ (τ = 0).

σ	Percentage of Agents Starting Their Evacuation		
	50%	**95%**	**99%**
1.0	1.2	2.4	3.0
2.0	2.4	4.9	6.1
4.0	4.7	9.8	12.1
8.0	9.4	19.6	24.3

3.5. Vehicular Movement

Vehicular movement is based on the classic car-following model [42] and general motor model equation [43,44], as in Equation (3).

$$a_{n+1}^{t+\delta t} = \left[\frac{\alpha_{l,m} \left(v_{n+1}^{t} \right)^{m}}{\left(x_{n}^{t} - x_{n+1}^{t} \right)^{l}} \right] \left(v_{n}^{t} - v_{n+1}^{t} \right) \quad (3)$$

where:

x_n^t = The location of the leading vehicle at time t
v_n^t = The speed of the leading vehicle
x_{n+1}^t = The location of the following vehicle at time t
v_{n+1}^t = The speed of the following vehicle at time t
l = The distance exponent (−1 to +4)
m = The speed exponent (−2 to +2)
$\alpha_{l,m}$ = The sensitivity coefficient
δt = The perception-reaction time

The parameters are adjustable and can be calibrated using empirical data. In an emergency, drivers tend to be more alert and responsive; thus, the perception-reaction time should be lower than usual. Therefore, the perception-reaction time for evacuation by car and motorcycle, in this case, is assumed to be reasonably close to zero.

Greenshield's model is used due to its relative simplicity and accuracy in developing a model of uninterrupted traffic that predicts and explains the trends observed in real traffic flows. The model assumes that under uninterrupted flows, speed and density are linearly related. However, due to the lack of empirical data from a real situation in the study area to set the parameters, the following parameters are set in this simulation: l is set to +2, m and δt are set to 0, and α is set to 369.44 m^2/s for cars and 69.44 m^2/s for motorcycles. Below is the derivation of parameter α, shown in Equations (4)–(13).

$$a_{n+1}^{t+\delta t} = \left[\frac{\alpha_{l,m}\left(v_{n+1}^{t}\right)^{m}}{\left(x_{n}^{t} - x_{n+1}^{t}\right)^{l}}\right]\left(v_{n}^{t} - v_{n+1}^{t}\right) \tag{4}$$

$$\ddot{x}_{n+1}^{t} = \left[\frac{\alpha_{2,0}}{\left(x_{n}^{t} - x_{n+1}^{t}\right)^{2}}\right]\left(\dot{x}_{n}^{t} - \dot{x}_{n+1}^{t}\right) \tag{5}$$

Let $h = \left(x_{n}^{t} - x_{n+1}^{t}\right)$; then, Equation (5) will have:

$$\ddot{x}_{n+1}^{t} = \left[\frac{\alpha_{2,0}}{h^2}\right]\frac{dh}{dt} \tag{6}$$

$$\frac{dv}{dt} = \left[\frac{\alpha_{2,0}}{h^2}\right]\frac{dh}{dt} \tag{7}$$

$$\int dv = \int \frac{\alpha_{2,0}}{h^2} dh \tag{8}$$

$$v = -\frac{\alpha_{2,0}}{h^2} + c \tag{9}$$

Plugging in the boundary conditions for the jammed state and free-flow state, we have:

$$\alpha K_j = c \tag{10}$$

$$\alpha = \frac{V_f}{K_j} \tag{11}$$

where α is estimated based on (K_j) as the jam density and (V_f) as the free-flow speed. The jam density for cars is set to 33 veh/km, 32 veh/km, and 28 veh/km in Padang city [45]. This jam density is used as a reference for the Panimbang case, and 30 veh/km is chosen as the jam density. The jam density for motorcycles is set to 120 veh/km, with a simple ratio (1:4) of the motorcycle dimension to the car dimension. The free-flow speed in Panimbang is also assumed to be 40 km/h for cars and 30 km/h for motorcycles. The α (sensitivity coefficient) values for cars and motorcycles are estimated as follows.

$$\alpha = 1.33\ km^2/h = 369.44\ m^2/s \ \rightarrow \ \text{Cars} \tag{12}$$

$$\alpha = 0.25\ km^2/h = 69.44\ m^2/s \ \rightarrow \ \text{Motorcycles} \tag{13}$$

The sensitivity coefficient in the model correlates to the acceleration and deceleration of vehicle movement calculated from the car-following model. It is shown that α = 369.44 m^2/s for cars leads to accelerations in the range of 5.155–10.31 m^2/s and decelerations in the range of 10.31–25.44 m^2/s. In the case of motorcycles, α = 69.44 m^2/s leads to accelerations in the range of 0.969–1.938 m^2/s and decelerations in the range of 1.938–4.782 m^2/s.

3.6. Pedestrian Movement

Walking speed is generally classified into various groups depending on inhabitants' age as a pedestrian speed variable. Based on Lee et al. (2015) [46], pedestrians are divided into three different types: children, adults, and elderly individuals, with walking speeds of 0.808 m/s, 1.111 m/s, and 0.772 m/s, respectively (Table 3). The physical conditions in the evacuation process, such as tiredness or stamina, and topography are not considered in this

study. In the simulation, all agents begin to evacuate by foot to their nearest road. Under this condition, agents who make different decisions are separated. The time required to access their cars for agents who choose not to evacuate by foot is assumed to be modelled by their milling time.

Table 3. Agent walking speeds considered in the simulation.

Age	Reference [46]		This Study	
	Walking Speed		Walking Speed	
	(km/h)	(m/s)	(km/h)	(m/s)
0–4	~	~		
5–9	2.17	0.603	2.91	0.808
10–14	3.39	0.942		
15–49	4.00	1.111	4.00	1.111
50–64	3.40	0.944		
65–74	2.82	0.783	2.78	0.772
75+	2.51	0.697		

4. Results

4.1. Transportation Mode Choice

Five types of transportation modes, walking, travelling by car, and travelling by motorcycle, with walking being divided into children, adults, and elderly individuals, are considered. The transportation mode choice test was divided into 11 mode choices as described (Table 1).

Figure 4 represents the correlation between the transportation mode choice and the mortality rate. It shows that the mortality rate decreases by approximately half as vehicle use increases. Motorcycles and cars contribute the least to the percentage of total deaths.

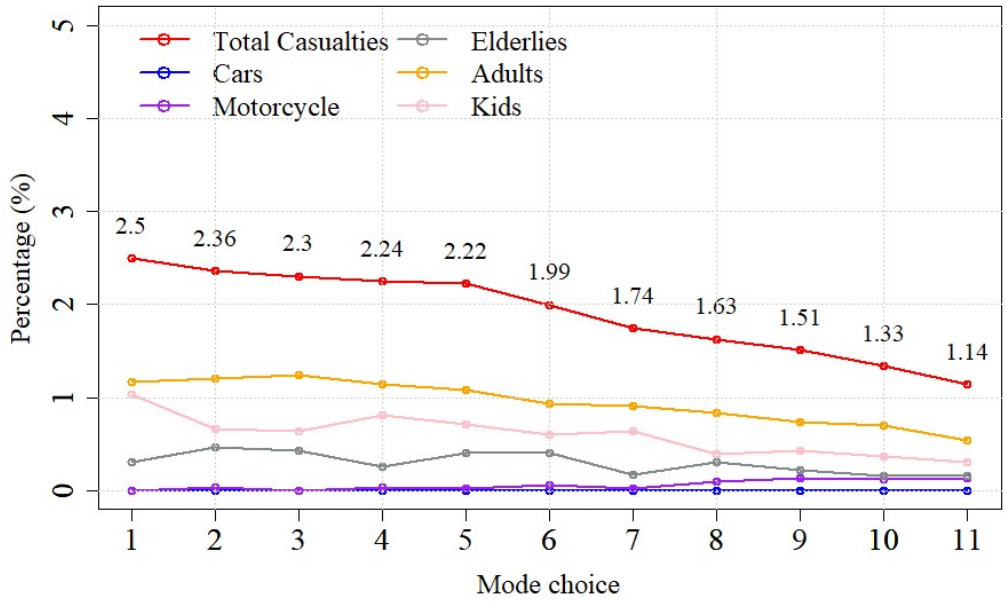

Figure 4. Total deaths (%) depending on the transportation mode choice as in Table 1.

In Figure 5, the casualties varied based on transportation mode. The locations of agents who decide to evacuate by car, by motorcycle, or by foot are not always the same, such that agent decision-making will change with the repetition of simulation runs.

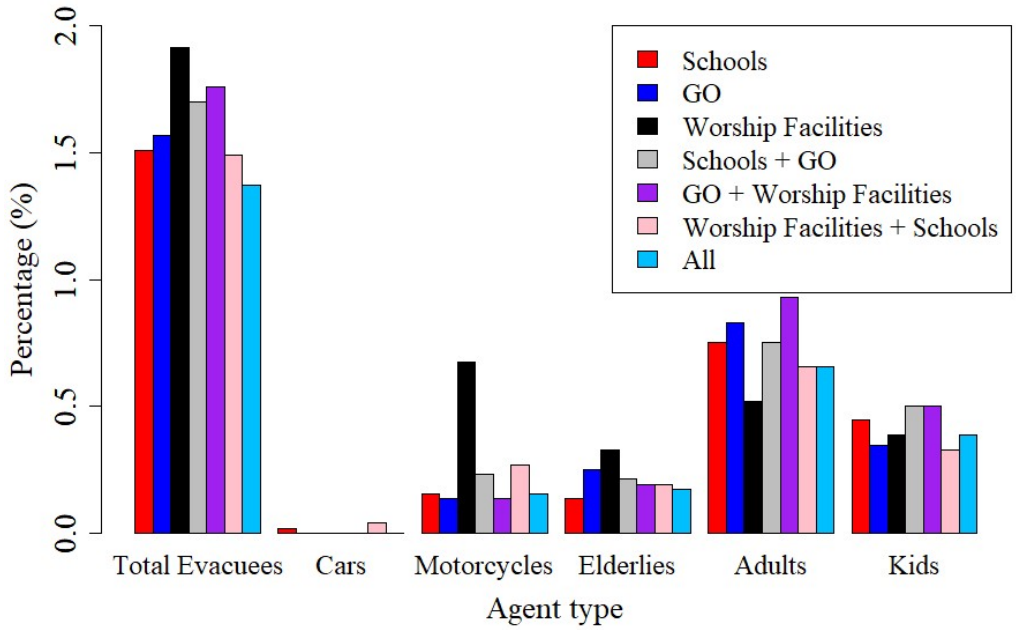

Figure 5. Total deaths (%) depending on the shelter choice.

4.2. Shelter Choice

There are 14 schools, 10 worship facilities, and 9 government offices (GOs) in the study area considered as shelters. In the shelter choice analysis, the effects of a single shelter choice and a combination shelter choice (i.e., evacuate to the closer shelter) on the casualty percentage are analysed. In the shelter choice test, several parameters are set as constants, such as mode choice 11 (50% vehicle use) for transportation, a delay time of 10 min, a scale parameter of 1.65, an average speed of cars of 40 km/h, and an average speed of motorcycles of 30 km/h. As described, all shelters were assumed to have an unlimited capacity, implying that agents consider only the shortest and most optimum path to a shelter from their initial location.

Figure 5 shows that as a single shelter choice, worship facilities have the highest mortality rate, 1.915%, followed by the combination choice of government offices and worship facilities, 1.76%. The use of all shelters has a casualty of 1.37%, and it reduces the mortality rate by approximately 0.5–0.6% compared to worship facilities as a single shelter choice. Agents who choose to evacuate by car contributed the lowest percentage to the mortality rate since the agents can evacuate faster to shelters by car.

4.3. Scale Parameter

The scale parameter or variations in departure time is one of the main attributes of the agent decision-making time discussed in the milling time. The larger σ is, the larger the tail of the later departure time distribution. It is difficult to make any specific value of the scale parameter to represent the actual situation because, in a real situation, many factors can affect the value, such as people's activities, whether it is day or night, and people's educational background.

In this study, a test was conducted to assess the correlation between the variations in the departure time of evacuees and the casualty percentages. The results of this test are based on the average values of five simulation runs. The delay time is constant with $\tau = 10$ min and transportation mode choice 11. Then, the scale parameter varies with 0, 1, 2, 4, 8, and 16. Figure 6 shows that casualties significantly increase as the scale parameter increases. The casualty percentages increase by approximately 0.6% from $\sigma = 0$ to $\sigma = 2$, and the effect of variations in departure time becomes more significant at $\sigma = 16$. The increase in the scale parameter becomes a crucial factor in the mortality rate because when $\sigma = 16$,

it increases more than two times to 2.77%, compared to 1.28% when σ = 0, meaning that variations in departure time have a significant impact on the mortality rate.

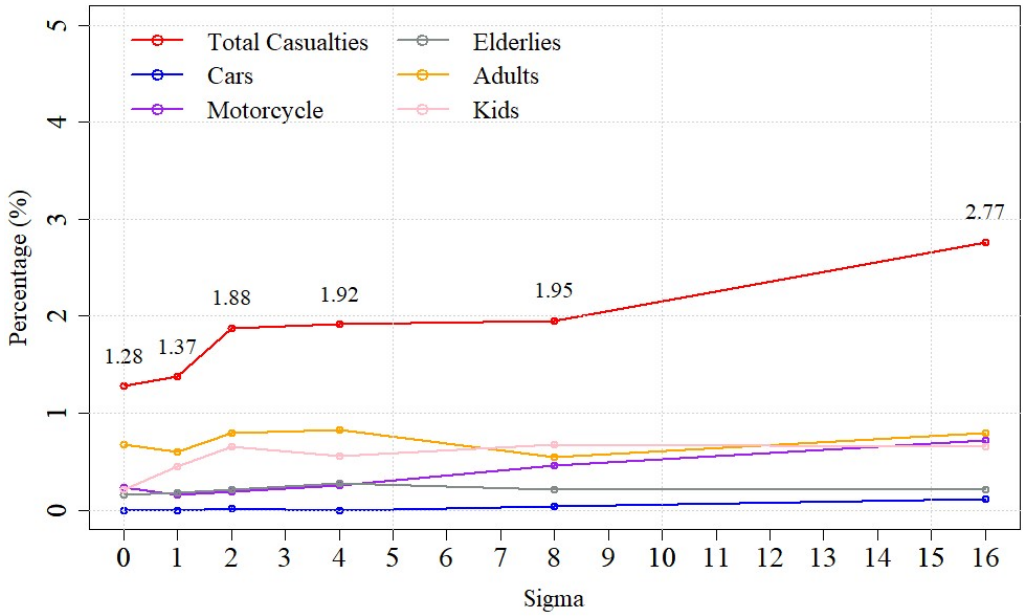

Figure 6. Mortality rate according to the varying scale parameters.

4.4. Scenario Analysis

As discussed, τ (delay time) is one of the parameters that affect agent decision-making time. No agents evacuate when t < τ. In a real situation, τ can vary based on many aspects, such as educational level, knowledge, and evacuation choice.

Figure 7 shows the tsunami timeline and scenario-based delay time in this study. The tsunami timeline is based on the Marina Jambu tide gauge data [26]. The tsunami arrived at the shoreline 32 min after the volcanic eruption. The first peak of the tsunami is 0.7 m 34 min after the eruption and reaches the maximum wave height of 1.35 m 39 min after the eruption. Seven scenarios were tested, starting with scenario 1 of τ = 0 min, i.e., immediate evacuation. In scenario 2, it was assumed that the tsunami warning signalled 10 min after the eruption, and agents started their evacuation process at τ = 10. Scenarios 3 to 5 assumed delay times of τ = 15, 20, and 25 min, respectively. In scenario 6, agents were assumed to start their evacuation while the tsunami arrived at the coastline. At the delay time τ = 39 min, in which the tsunami reached the maximum wave height, scenario 7 was conducted.

Figure 8 presents the percentage of evacuees from the seven scenario simulations with a constant scale parameter (σ = 1.65) and transportation mode choice 11. The total number of evacuees decreases as the delay time or preparation time increases. In the first scenario, where agents perform an immediate evacuation, the total percentage of evacuees is the highest, 95.9%, and decreases by approximately 14–15% in the last scenario where agents start their evacuation when the tsunami reaches its maximum wave height. The motorcycle mode choice and adults depict a larger gradient decrease in scenario 6 with τ = 32 min.

Figure 9 presents the effect of the delay time on the mortality rate. The mortality rate increases significantly as the delay time increases, except in scenario 7. The mortality rate in scenario 7, 2.96%, is lower than that in scenarios 5 and 6. The mortality rate varies in each scenario, mainly because of the locations of agents who are randomly distributed in each run. In this test, cars contributed the lowest percentage of the mortality rate, indicating that it is a very effective evacuation mode choice. The main reason for the lower mortality rate in scenario 7 than in scenarios 5 and 6 is that the initial locations of agents in scenario 7 are higher than those in scenarios 5 and 6. Moreover, in scenario 7, agents are evacuating when the tsunami is retreating seaward, while in scenarios 5 and 6, agents are evacuating when the tsunami propagates inland with increasing height.

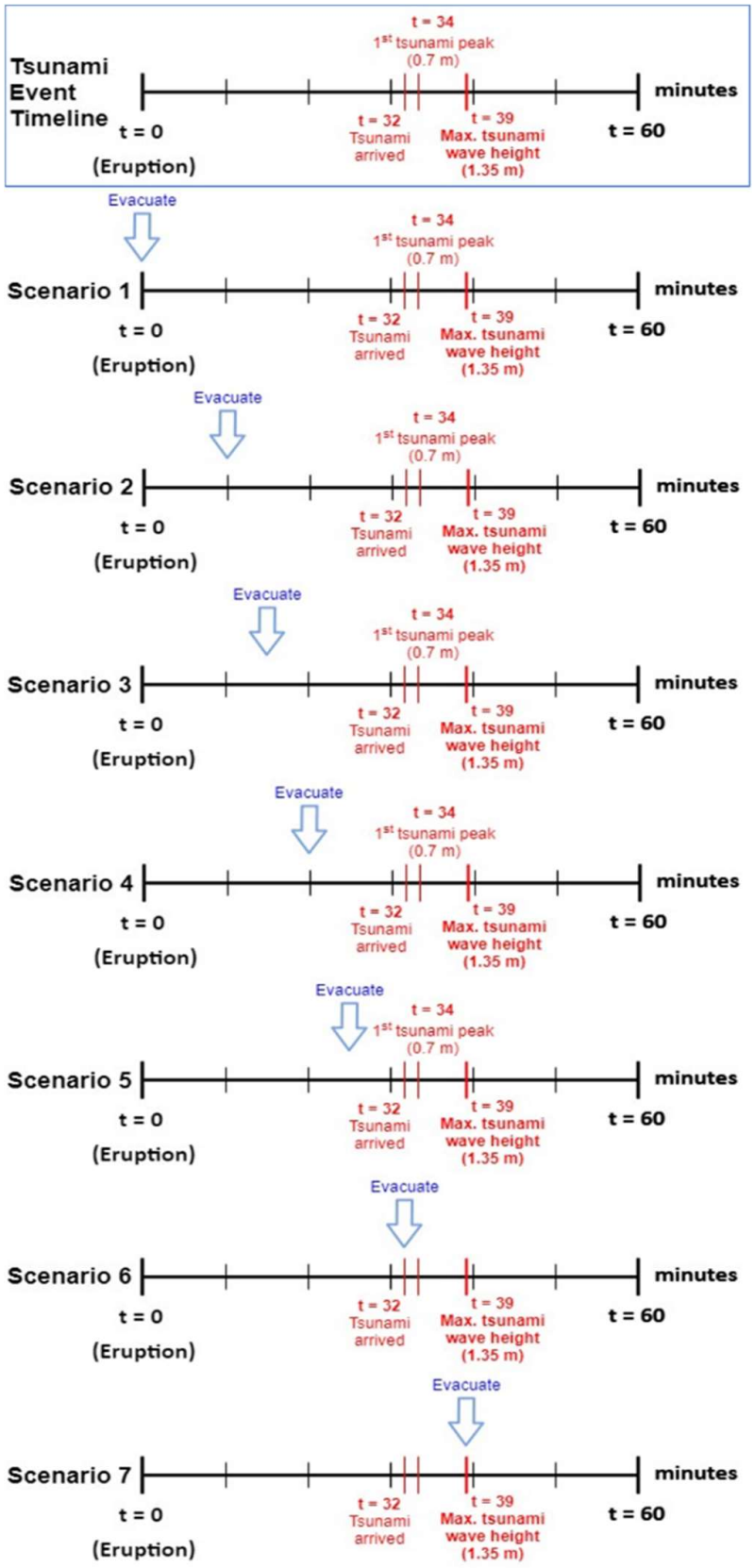

Figure 7. Tsunami event timeline and seven simulation scenarios with different delay times.

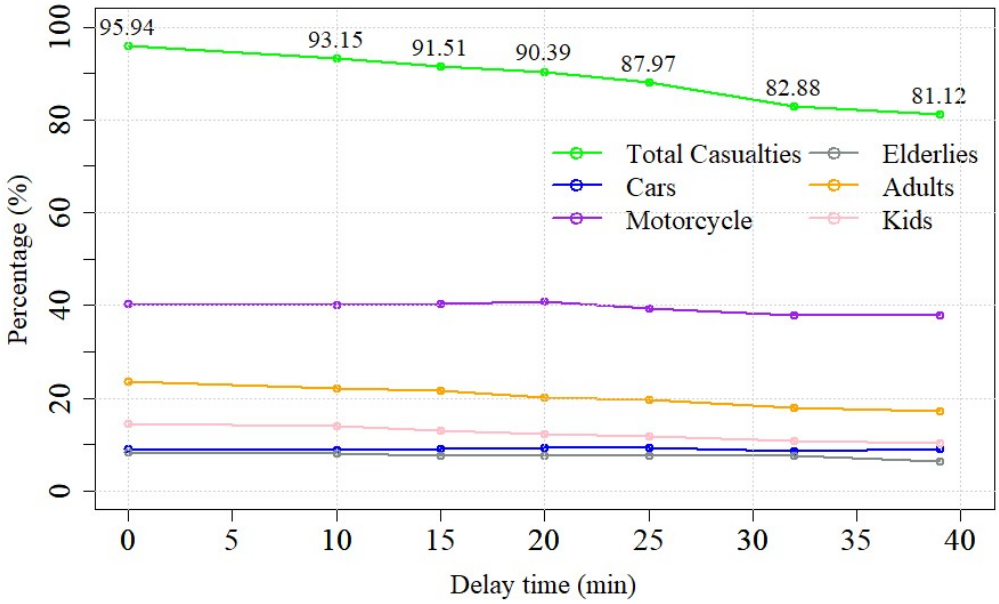

Figure 8. Resulting evacuees (%) depending on the delay time, τ (min).

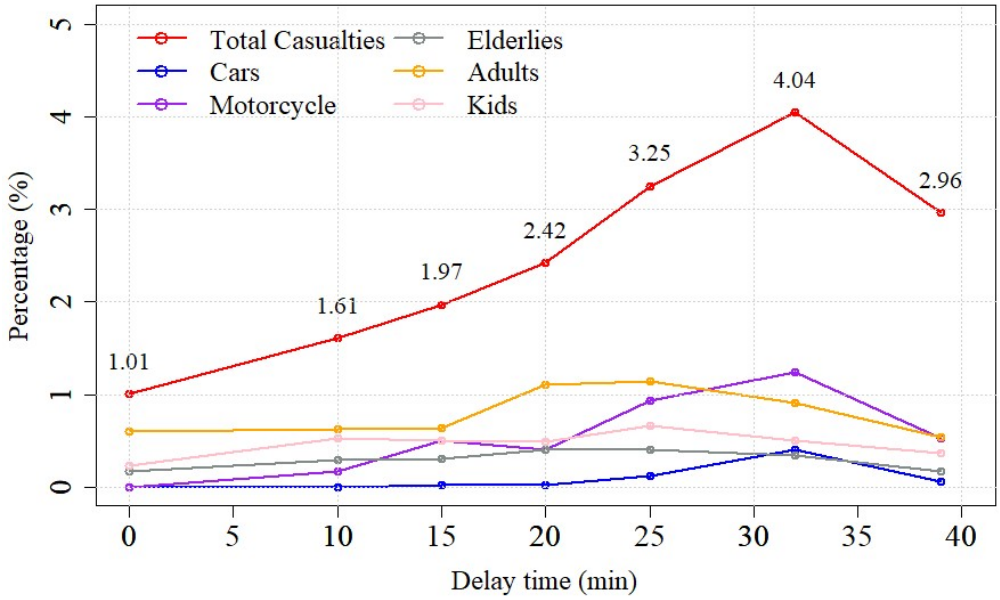

Figure 9. Resulting casualties (%) depending on the delay time, τ (min).

4.5. Tsunami Risk Hot Spots

To propose and evaluate the effects of tsunami shelters in the Panimbnag area, tsunami risk hot spots were estimated based on the results of scenario analysis. The result of the worst case, scenario 6, is presented in Figure 10 with the locations of casualties. Most of the casualties and hot spots are found in the eastern Panimbang region, where the population density is high. Furthermore, the tsunami hazard map in the Panimbang area is assessed using GIS-based multicriteria analysis. The physical criteria considered are elevation, slope, distance from the shoreline, and distance from riverbanks. Next, weights for each criterion and class scores to produce tsunami hazard levels in the study area are implemented from [47,48], as shown in Table 4. The distance from the shoreline is based on the MSL.

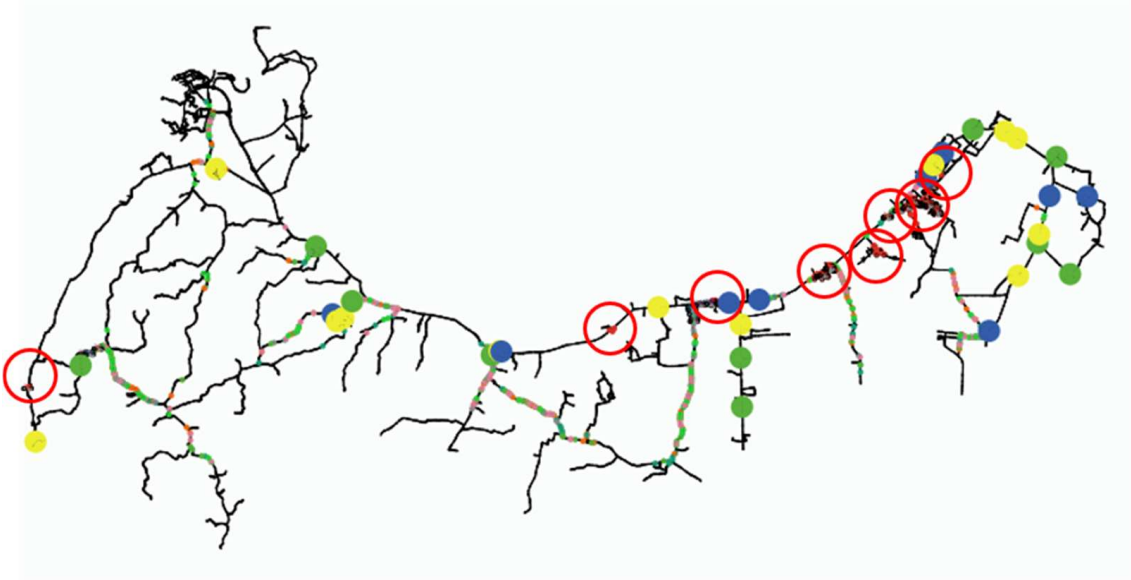

Figure 10. Casualty locations are highlighted in red circles based on the result of scenario 6, the worst-case scenario in terms of the number of casualties.

Table 4. Scores and weights for tsunami disaster hazard criteria.

Criteria	Class	Score	Weight
Distance from the shoreline (m)	0–500 m	5	30
	501–1000 m	4	
	1001–1500 m	3	
	1501–3000 m	2	
	>3000 m	1	
Elevation (m)	<10 m	5	30
	11–25 m	4	
	26–50 m	3	
	51–100 m	2	
	>100 m	1	
Slope (%)	0–2%	5	25
	3–5%	4	
	6–15%	3	
	16–40%	2	
	>40%	1	
Distance from rivers (m)	0–100 m	5	15
	101–200 m	4	
	201–300 m	3	
	301–500 m	2	
	>500 m	1	

In the GIS-based spatial overlaying analysis, the hazard score N is calculated using Equations (14) and (15) by using those weights and scores for each criterion and class [49].

$$N = \sum(B_i \times S_i) \tag{14}$$

where B_i is the weight of each criterion and S_i is the score of each class.

$$N = \left[(0.3 \times S_{shoreline}) + (0.3 \times S_{elev}) + \left(0.25 \times S_{slope}\right) + (0.15 \times S_{river})\right] \tag{15}$$

Figure 11 illustrates the tsunami hazard map resulting from the GIS-based spatial overlaying analysis. The tsunami hazard levels are divided into five levels, namely, very

low, low, moderate, high, and very high, based on the hazard scores [50,51]. To identify the locations of the VESs in the study area, the hazard map is combined with the locations of casualties, as shown in Figure 10. As a result, the vertical shelters in Figure 11 are proposed at the tsunami risk hot spots in high and very high tsunami risk zones.

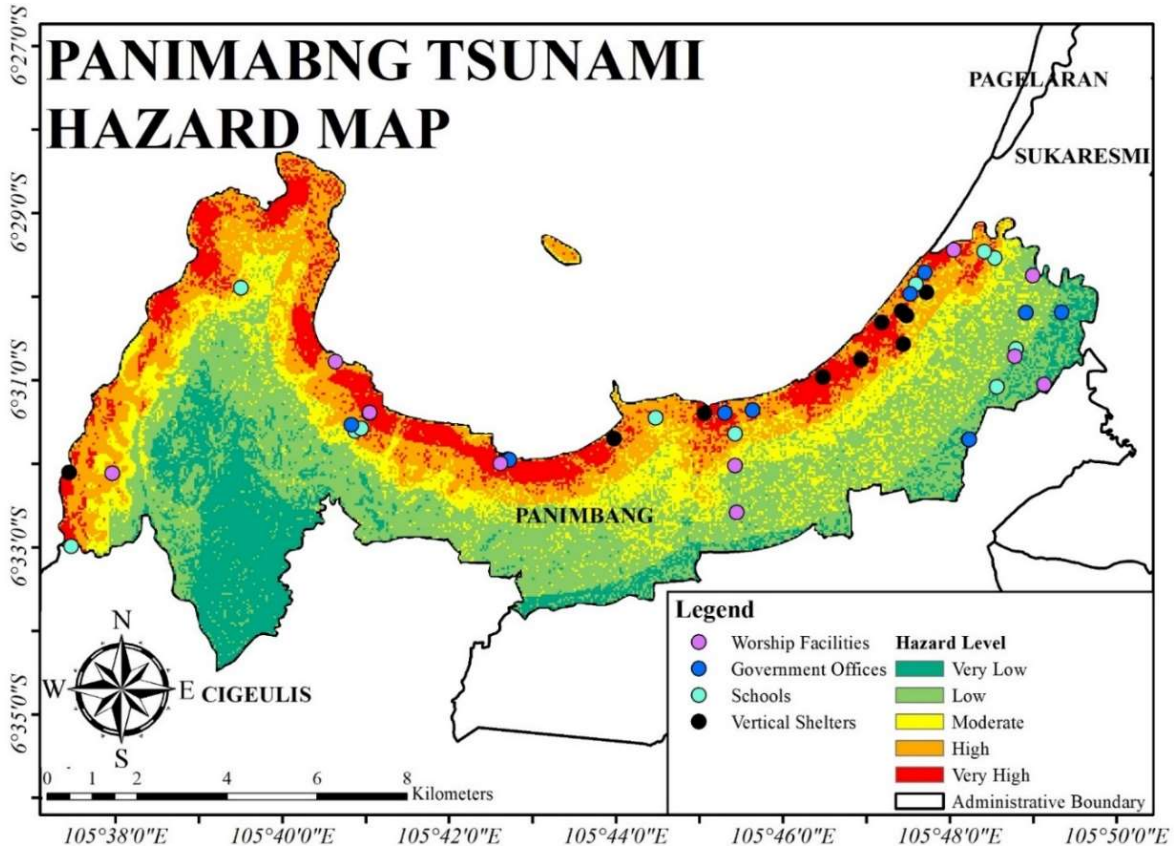

Figure 11. Panimbang tsunami hazard map and proposed locations of evacuation shelters.

5. Discussion

Effects of VESs

To investigate the effects of the proposed VESs in terms of evacuees and casualties, additional simulations were performed. Notably, it is assumed that the VES structures follow the design features from [28] with unlimited capacity.

In addition, in the simulations, the scale parameter is set to a constant (σ = 1.65) with transportation mode choice 11. The evacuation shelters used are a combination of 10 proposed VESs and HESs, including schools (14), worship facilities (10), and government offices (9). The additional simulation scenarios are based on the delay time in the agent decision-making time. It starts with the immediate evacuation, i.e., τ = 0 min, and then continues to τ = 10, 15, 20, and 25 min. At τ = 34 min, the tsunami arrives at the land area, and at τ = 39 min, the tsunami reaches its maximum wave height.

Figure 12a,b exhibit the total evacuee (%) resulting from the simulations with the VESs and HES combination and HESs only, respectively. The evacuees do not significantly increase compared to those of the HES-only simulation, except in the 6th scenario. At the immediate evacuation τ = 0 min, the increment in the evacuee percentage is approximately 1% and slightly increases by 0.2% in the 7th scenario. The 6th scenario result shows an impact on the evacuee percentage of approximately 3.5–4%. Figure 13a,b presents the casualty percentages of both simulations. Both simulation trends are analogous, except in the casualty percentage of the 3rd scenario in the VESs and HES simulations. As noted above, the casualty percentage is slightly increased compared to the 2nd scenario. In general, the effect of the proposed VESs on the simulation can decrease the casualty

percentage by 1.25–2 times, implying that adding VESs in high and very high tsunami risk areas has a significant effect on decreasing the mortality rate.

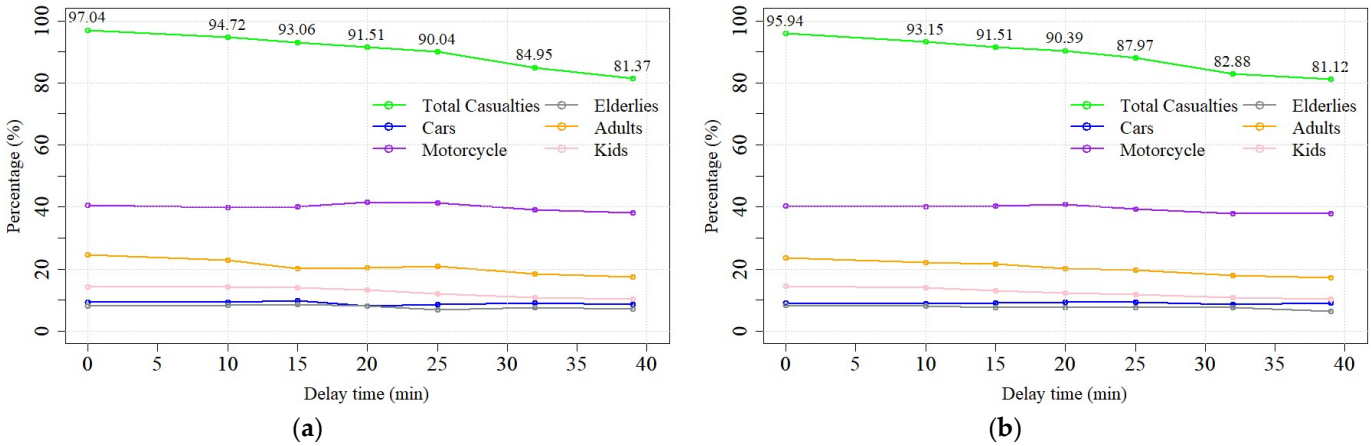

Figure 12. Comparison of the evacuee (%) from (**a**) the VESs and HES simulation and (**b**) the HES simulation.

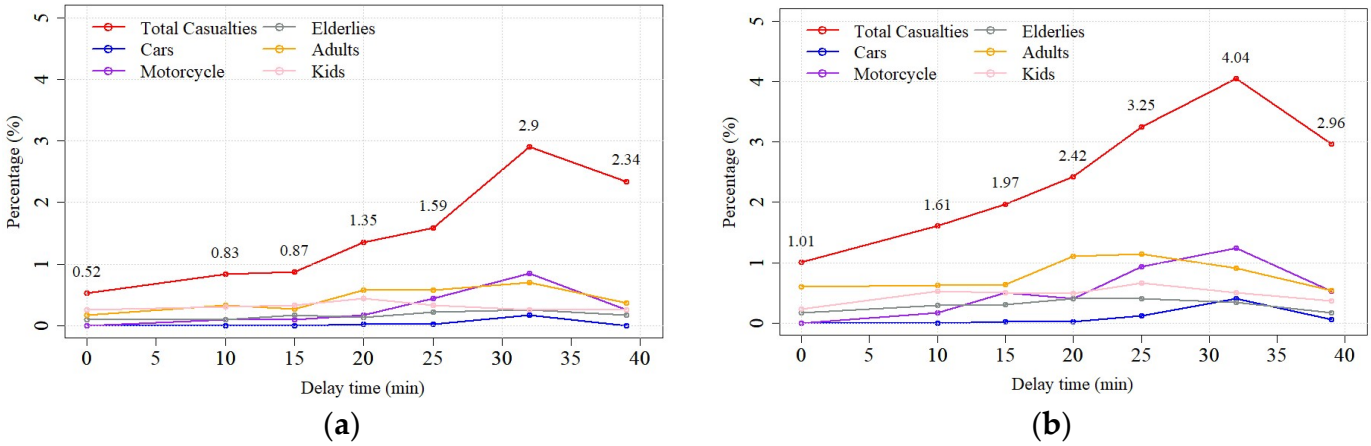

Figure 13. Comparison of the mortality rate from (**a**) the VESs and HES simulations and (**b**) the HES simulations.

6. Conclusions

This research presents a multimodal tsunami evacuation study using the ABM approach. The research objectives are related to the proposed shelters and how the variations in agent decision-making time, shelter choice, and transportation mode choice in an evacuation scenario impact the evacuee and mortality rates in the Panimbang subdistrict in Pandeglang, Banten, Indonesia. ABM using the NetLogo programming environment was applied to simulate and conduct sensitivity tests of the effect of various factors on the evacuee and casualty percentages. The effect of the proposed VESs in high tsunami risk areas on the mortality rates under various scenarios was also investigated. Based on the results of agent-based modelling, this study draws the following conclusions:

The transportation mode choice of vehicles significantly reduces the mortality rate, and cars are the effective mode choice for transportation in the study region.

Schools show the highest contribution to total evacuees among all existing single shelter choices, and multiple or all shelter choices can increase the number of evacuees.

The mortality rate is sensitive to the milling time represented by delay time τ and the variations in decision-making time σ.

Additionally, the tsunami hot spots based on the locations of casualties from the worst-case simulation and the tsunami hazard map are estimated based on GIS-based multicriteria

analysis. Based on the additional simulation results, the combination of VESs and HESs can decrease the casualty percentage by 1.25–2 times compared to that of HES-only results. The proposed VESs in the study area have a significant impact on decreasing the mortality rate.

In terms of the capacity limit of shelters, a certain capacity shelter will cause a longer evacuation time for agents because they have to travel for a longer period of time to find another shelter with spare capacity when the first shelter is full. Thus, it is likely to increase the mortality rate when considering the capacity limit of a shelter.

In the case of an underwater earthquake-driven tsunamis, earthquake and tsunami forces are also critical factors to consider in the evacuation process. For example, houses collapsed and damaged by the earthquake and tsunami forces would be negative obstacles in the evacuation process, causing an increase in the mortality rate.

Finally, this study has some limitations, such as the capacity of shelters as mentioned, the number of physical criteria in tsunami hazard mapping, and detailed interactions among agents. This should be considered in future works. However, it provides useful insights into the effects of tsunami shelters and choices during the evacuation process and will be the basic platform for an integrated disaster simulation system for an inundation, congestion, and evacuation process, such as that in Florida, FL, USA [52].

Supplementary Materials: The following are available online at https://www.mdpi.com/article/10.3390/jmse10081055/s1, Table S1. Historical data on tsunami disasters in Indonesia. 2018 Palau Tsunami and onwards are not considered. Table S2. Anak Krakatoa eruption-induced tsunami timeline; Figure S1. Panimbang population dataset (2018), divided by age group. (Source: ((Statistics Indo-nesia-Pandeglang District) BPS, 2018)); Figure S2. The tide gauge locations in Banten and Lampung Provinces; Figure S3. De-tided waveforms at Marina Jambu (Heidarzadeh et al., 2020). Figure S4. Casualty percentage in the 1st scenario (τ = 0 min), the 2nd scenario (τ = 10 min), the 3rd scenario (τ = 15 min), and the 4th scenario (τ = 20 min). References [24,27] are cited in the supplementary materials.

Author Contributions: Conceptualization, methodology, formal analysis, investigation, visualization, R.D.S. and H.S.L.; software, validation, writing—original draft preparation, R.D.S.; writing—review and editing, H.S.L. and C.F.; supervision, project administration, funding acquisition, H.S.L. All authors have read and agreed to the published version of the manuscript.

Funding: This research received no external funding.

Institutional Review Board Statement: Not applicable.

Informed Consent Statement: Not applicable.

Data Availability Statement: Not applicable.

Acknowledgments: The first author memorizes Byung Ho Choi from Sungkyunkwan University in Korea for his passion and enthusiasm for the education and research on coasts and seas, which is the legacy he left to his students. We share the good fortune and privilege to have had him as a dear teacher and colleague. The second author is supported by the JICA Innovative Asia Program.

Conflicts of Interest: The authors declare no conflict of interest.

References

1. Ashar, F.; Amaratunga, D.; Haigh, R. The Analysis of Tsunami Vertical Shelter in Padang City. *Procedia Econ. Financ.* **2014**, *18*, 916–923. [CrossRef]
2. Nurhayaty, A.; Wimbarti, S.; Triatmadja, R.; Hastjarjo, T.D. Model of Tsunami Preparedness for Indonesian Tsunami Prone Areas Communities. *J. Disaster Res.* **2015**, *10*, 957–965. [CrossRef]
3. Rogers, K. *Indonesia Disaster Reveals Community Preparedness Shortfalls*; Devex: Washington, DC, USA, 2018.
4. The Joint Committee of Indonesia and Japan on Disaster Reduction. *Building the Resilience of Indonesia and its Communities to Disasters for the Next Generation*; The Joint Committee of Indonesia and Japan on Disaster Reduction: Tokyo, Japan, 2006; p. 35.
5. Kodijat, A.M.; Rossel, B.A.; Julius, A.M.; Octonovrilna, L.; Cahyaningrum, A.P. Preserving past tsunami information for future preparedness in Indonesia and the Philippines. *MATEC Web Conf.* **2018**, *229*, 01016. [CrossRef]
6. Adiyoso, W.; Kanegae, H. The effect of different disaster education programs on tsunami preparedness among schoolchildren in Aceh, Indonesia. *Disaster Mitig. Cult. Herit. Hist. Cities* **2012**, *6*, 165–172.

7. Davis, J.R.; Paramygin, V.A.; Figueiredo, R.J.; Sheng, Y.P.; Vogiatzis, C.; Pardalos, P.M. *The Coastal Science Educational Virtual Appliance (CSEVA)*; ASCE: Reston, VA, USA, 2011; pp. 359–377.
8. LIPI (The Indonesian Institute of Sciences); BMKG (Meteorological, Climatological, and G.A., & BNPB (Indonesia National Geospatial Information Agency). *Information Guidebook Tsunami Early Warning for Broadcasting Institutions in Indonesia*; LIPI: Indonesia; BMKG: Indonesia, 2012.
9. Syamsidik; Benazir; Luthfi, M.; Suppasri, A.; Comfort, L.K. The 22 December 2018 Mount Anak Krakatau volcanogenic tsunami on Sunda Strait coasts, Indonesia: Tsunami and damage characteristics. *Nat. Hazards Earth Syst. Sci.* **2020**, *20*, 549–565. [CrossRef]
10. Usman, F.; Murakami, K.; Dwi Wicaksono, A.; Setiawan, E. Application of Agent-Based Model Simulation for Tsunami Evacuation in Pacitan, Indonesia. *MATEC Web Conf.* **2017**, *97*, 01064. [CrossRef]
11. Mas, E.; Koshimura, S.; Imamura, F.; Suppasri, A.; Muhari, A.; Adriano, B. Recent Advances in Agent-Based Tsunami Evacuation Simulations: Case Studies in Indonesia, Thailand, Japan and Peru. *Pure Appl. Geophys.* **2015**, *172*, 3409–3424. [CrossRef]
12. Yosritzal; Kemal, B.M.; Purnawan; Putra, H. An observation of the walking speed of evacuees during a simulated tsunami evacuation in Padang, Indonesia. *IOP Conf. Ser. Earth Environ. Sci.* **2018**, *140*, 012090. [CrossRef]
13. Lämmel, G.; Rieser, M.; Nagel, K.; Taubenböck, H.; Strunz, G.; Goseberg, N.; Schlurmann, T.; Klüpfel, H.; Setiadi, N.; Birkmann, J. Emergency Preparedness in the Case of a Tsunami—Evacuation Analysis and Traffic Optimization for the Indonesian City of Padang. In *Pedestrian and Evacuation Dynamics 2008*; Klingsch, W.W.F., Rogsch, C., Schadschneider, A., Schreckenberg, M., Eds.; Springer: Berlin/Heidelberg, Germany, 2010; pp. 171–182.
14. Wafda, F.; Saputra, R.W.; Nurdin, Y.; Nasaruddin; Munadi, K. Agent-based tsunami evacuation simulation for disaster education. In Proceedings of the International Conference on ICT for Smart Society, Jakarta, Indonesia, 13–14 June 2013; pp. 1–4.
15. Goto, Y.; Muzailin, A.; Agussabti; Yudha, N.; Diyah, K.Y.; Ardiansyah. Tsunami Evacuation Simulation for Disaster Education and City Planning. *J. Disaster Res.* **2012**, *7*, 92–101. [CrossRef]
16. Paris, A.; Heinrich, P.; Paris, R.; Abadie, S. The December 22, 2018 Anak Krakatau, Indonesia, Landslide and Tsunami: Preliminary Modeling Results. *Pure Appl. Geophys.* **2020**, *177*, 571–590. [CrossRef]
17. Takabatake, T.; Shibayama, T.; Esteban, M.; Achiari, H.; Nurisman, N.; Gelfi, M.; Tarigan, T.A.; Kencana, E.R.; Fauzi MA, R.; Panalaran, S. Field survey and evacuation behaviour during the 2018 Sunda Strait tsunami. *Coast. Eng. J.* **2019**, *61*, 423–443. [CrossRef]
18. Ren, Z.; Wang, Y.; Wang, P.; Hou, J.; Gao, Y.; Zhao, L. Numerical study of the triggering mechanism of the 2018 Anak Krakatau tsunami: Eruption or collapsed landslide? *Nat. Hazards* **2020**, *102*, 1–13. [CrossRef]
19. Suwarsono Nf Prasasti, I.; Nugroho, J.T.; Sitorus, J.; Triyono, D. Detecting the lava flow deposits from 2018 Anak Krakatau eruption using data fusion Landsat-8 optic and Sentinel-1 SAR. *Int. J. Remote Sens. Earth Sci.* **2019**, *15*, 157–166.
20. Maeno, F.; Imamura, F. Tsunami generation by a rapid entrance of pyroclastic flow into the sea during the 1883 Krakatau eruption, Indonesia. *J. Geophys. Res. Solid Earth* **2011**, *116*, B09205. [CrossRef]
21. Kimata, F.; Pamitro, Y.E.; Abidin, H.Z. Understanding the 2007–2008 eruption of Anak Krakatau Volcano by combining remote sensing technique and seismic data. *Int. J. Appl. Earth Obs. Geoinf.* **2012**, *14*, 73–82.
22. BNPB (Indonesia National Geospatial Information Agency). *Indonesia Tsunami Historical Data*; BNPB: Cibinong, Indonesia, 2019. Available online: https://bnpb.go.id/ (accessed on 15 November 2020).
23. BNPB (Indonesia National Geospatial Information Agency). *The Sunda Strait Tsunami, Update on 13 January 2019*; BNPB: Cibinong, Indonesia, 2019. Available online: https://bnpb.go.id/ (accessed on 30 November 2020).
24. BPS (Statistics Indonesia—Pandeglang District). *Pandeglang Dalam Angka*; BPS: Central Jakarta, Indonesia, 2018.
25. BPS (Statistics Indonesia). Number of Motor Vehicles by Types, Indonesia 1949–2018. In *Statistics Indonesia*; Statistics Indonesia: Central Jakarta, Indonesia, 2019. Available online: https://www.bps.go.id/linkTableDinamis/view/id/1133 (accessed on 30 November 2020).
26. Heidarzadeh, M.; Ishibe, T.; Sandanbata, O.; Muhari, A.; Wijanarto, A.B. Numerical modeling of the subaerial landslide source of the 22 December 2018 Anak Krakatoa volcanic tsunami, Indonesia. *Ocean. Eng.* **2020**, *195*, 106733. [CrossRef]
27. Sithole, G.; Vosselman, G. Experimental comparison of filter algorithms for bare-Earth extraction from airborne laser scanning point clouds. *ISPRS J. Photogramm. Remote Sens.* **2004**, *59*, 85–101. [CrossRef]
28. FEMA. *Guidelines for Design of Structures for Vertical Evacuation from Tsunamis*; US Department of Homeland Security, Federal Emergency Management Agency: Washington, DC, USA, 2009.
29. Rojahn, C.; Heintz, J.A.; Hortacsu, A.; Clark, J.L.; Ewing, L.; Goltz, J.D.; Holmes, W.T.; Petty, E.; Priest, G.; Turner, A. *Vertical Evacuation from Tsunamis: A Guide for Community Officials*; Federal Emergency Management Agency: Washington, DC, USA, 2009.
30. Wang, H.; Mostafizi, A.; Cramer, L.A.; Cox, D.; Park, H. An agent-based model of a multimodal near-field tsunami evacuation: Decision-making and life safety. *Transp. Res. Part C Emerg. Technol.* **2016**, *64*, 86–100. [CrossRef]
31. Yeh, H. Gender and age factors in tsunami casualties. *Nat. Hazards Rev.* **2010**, *11*, 29–34. [CrossRef]
32. Wilensky, U. *NetLogo*; Center for Connected Learning and Computer-Based Modeling, Northwestern University: Evanston, IL, USA, 1999.
33. Mostafizi, A.; Wang, H.; Cox, D.; Dong, S. An agent-based vertical evacuation model for a near-field tsunami: Choice behavior, logical shelter locations, and life safety. *Int. J. Disaster Risk Reduct.* **2019**, *34*, 467–479. [CrossRef]
34. Dijkstra, E.W. A note on two problems in connexion with graphs. *Numer. Math.* **1959**, *1*, 269–271. [CrossRef]

35. Jungnickel, D. The Greedy Algorithm. In *Graphs, Networks and Algorithms*; Jungnickel, D., Ed.; Springer: Berlin/Heidelberg, Germany, 1999; pp. 129–153.
36. Sudhakara, P.; Ganapathy, V. Trajectory planning of a mobile robot using enhanced A-star algorithm. *Indian J. Sci. Technol.* **2016**, *9*, 1–10. [CrossRef]
37. Mostafizi, A.; Wang, H.; Cox, D.; Cramer, L.A.; Dong, S. Agent-based tsunami evacuation modeling of unplanned network disruptions for evidence-driven resource allocation and retrofitting strategies. *Nat. Hazards* **2017**, *88*, 1347–1372. [CrossRef]
38. Mostafizi, A. Agent-Based Tsunami Evacuation Model: Life Safety and Network Resilience. Master's. Thesis, Oregon State University, Corvallis, OR, USA, 2016.
39. National Research Council. *Facing Hazards and Disasters: Understanding Human Dimensions*; National Academies Press: Washington, DC, USA, 2016.
40. Lindell, M.; Prater, C. Critical Behavioral Assumptions in Evacuation Time Estimate Analysis for Private Vehicles: Examples from Hurricane Research and Planning. *J. Urban Plan. Dev.* **2007**, *133*, 18–29. [CrossRef]
41. Mas, E.; Supassri, A.; Imamura, F.; Koshimura, S. Agent-based Simulation of the 2011 Great East Japan Earthquake/Tsunami Evacuation: An Integrated Model of Tsunami Inundation and Evacuation. *J. Nat. Disaster Sci.* **2012**, *34*, 41–57. [CrossRef]
42. Brackstone, M.; McDonald, M. Car-following: A historical review. *Transp. Res. Part F Traffic Psychol. Behav.* **1999**, *2*, 181–196. [CrossRef]
43. Herman, R.; Montroll, E.W.; Potts, R.B.; Rothery, R.W. Traffic dynamics: Analysis of stability in car following. *Oper. Res.* **1959**, *7*, 86–106. [CrossRef]
44. Ahmed, H.U.; Huang, Y.; Lu, P. A Review of Car-Following Models and Modeling Tools for Human and Autonomous-Ready Driving Behaviors in Micro-Simulation. *Smart Cities* **2021**, *4*, 314–335. [CrossRef]
45. Gunawan, H.; Ruslinda, Y.; Putri, D. Pengaruh Karakteristik Lalu Lintas terhadap Konsentrasi Gas NO_2 di Udara Ambien Roadside Jaringan Jalan Sekunder Kota Padang. In Proceedings of the Andalas Civil Engineering (ACE) Conference, Padang, Indonesia, 13–14 August 2015.
46. Lee, S.H.; Goo, S.H.; Chun, Y.W.; Park, Y.J. The Spatial Location Analysis of Disaster Evacuation Shelter for Considering Resistance of Road Slope and Difference of Walking Speed by Age—Case Study of Seoul, Korea. *J. Korean Soc. Geospat. Inf. Syst.* **2015**, *23*, 69–77. [CrossRef]
47. Faiqoh, I.; Gaol, J.L.; Ling, M.M. Vulnerability Level Map of Tsunami Disaster in Pangandaran Beach, West Java. *Int. J. Remote Sens. Earth Sci.* **2013**, *10*, 90–103. [CrossRef]
48. Hadi, F.; Damayanti, A. Aplikasi Sig Untuk Pemetaan Zona Keterpaparan Permukiman Terhadap Tsunami. *Semin. Nas. Geomatika* **2018**, *2*, 317–324. [CrossRef]
49. Muzaki, A.A. Spatial Analysis of Reef Ecosystem Based of the Marine Conservation Using Cell Based Modelling Method in Seribu Island, DKI Jakarta. Ph.D. Thesis, Bogor Agricultural University, Bogor, Indonesia, 2008.
50. Cabrera, J.; Lee, H.S. Flood risk assessment for Davao Oriental in the Philippines using geographic information system-based multi-criteria analysis and the maximum entropy model. *J. Flood Risk Manag.* **2020**, *13*, e12607. [CrossRef]
51. Cabrera, J.; Lee, H.S. Flood risk assessment using GIS-based multi-criteria analysis: A case study in Davao Oriental, Philippines. *Water* **2019**, *11*, 2203. [CrossRef]
52. Davis, J.R.; Paramygin, V.A.; Vogiatzis, C.; Sheng, Y.P.; Pardalos, P.M.; Figueiredo, R.J. Strengthening the Resiliency of a Coastal Transportation System through Integrated Simulation of Storm Surge, Inundation, and Nonrecurrent Congestion in Northeast Florida. *J. Mar. Sci. Eng.* **2014**, *2*, 287–305. [CrossRef]